JACS
JOURNAL OF THE AMERICAN CHEMICAL SOCIETY

ARTICLE

pubs.acs.org/JACS

Complete Budding and Asymmetric Division of Primitive Model Cells To Produce Daughter Vesicles with Different Interior and Membrane Compositions

Meghan Andes-Koback and Christine D. Keating*

Department of Chemistry, Pennsylvania State University, University Park, Pennsylvania 16802, United States

Supporting Information

ABSTRACT: Asymmetric cell division is common in biology and plays critical roles in differentiation and development. Unicellular organisms are often used as model systems for understanding the origins and consequences of asymmetry during cell division. Although basic as compared to mammalian cells, these are already quite complex. We report complete budding and asymmetric fission of very simple nonliving model cells to produce daughter vesicles that are chemically distinct in both interior and membrane compositions. Our model cells are based on giant lipid vesicles (GVs, 10−30 μm) encapsulating a polyethylene glycol (PEG)/dextran aqueous two-phase system (ATPS) as a crowded and compartmentalized cytoplasm mimic. Ternary lipid compositions were used to provide coexisting micrometer-scale liquid disordered (L_d) and liquid ordered (L_o) domains in the membranes. ATPS-containing vesicles formed buds when sucrose was added externally to provide increased osmotic pressure, such that they became not only morphologically asymmetric but also asymmetric in both their interior and their membrane compositions. Further increases in osmolality drove formation of two chemically distinct daughter vesicles, which were in some cases connected by a lipid nanotube (complete budding), and in others were not (fission). In all cases, separation occurred at the aqueous−aqueous phase boundary, such that one daughter vesicle contained the PEG-rich aqueous phase and the other contained the dextran-rich aqueous phase. PEGylated lipids localized in the L_o domain resulted in this membrane domain preferentially coating the PEG-rich bud prior to division, and subsequently the PEG-rich daughter vesicle. Varying the mole ratio of lipids resulted in excess surface area of L_o or L_d membrane domains such that, upon division, this excess portion was inherited by one of the daughter vesicles. In some cases, a second "generation" of aqueous phase separation and budding could be induced in these daughter vesicles. Asymmetric fission of a simple self-assembled model cell, with production of daughter vesicles that harbored different protein concentrations and lipid compositions, is an example of the seemingly complex behavior possible for simple molecular assemblies. These compartmentalized and asymmetrically dividing ATPS-containing GVs could serve as a test bed for investigating possible roles for spatial and organizational cues in asymmetric cell division and inheritance.

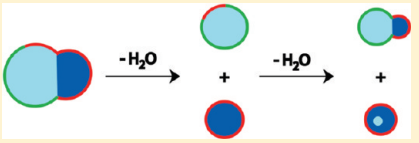

INTRODUCTION

An individual biological cell is the smallest living entity, and yet even the simplest living cells are overwhelmingly complex. Model cells designed to mimic one or more key aspects of their biological counterparts are therefore very attractive as a route to understand the chemical and physical basis of cell structure and function. Lipid vesicles have long been used as models for the membranes of biological cells.[1,2] They are simple to prepare and enable the lipid composition to be varied as desired for fundamental studies of membrane biophysics. Giant vesicles (GVs), which are defined as those having diameters greater than a micrometer,[1−5] are of particular interest because they are on the same scale as living cells and are amenable to fluorescence optical microscopy. Important insights into the role of lipid composition in, for example, transmembrane diffusion, membrane mechanical properties, and lipid phase separation have been gained from such studies.[2,6,7] Remarkable morphological transformations including vesicle fusion, budding, and fission have been observed in these model membranes.[8−15]

A wide variety of molecules and materials have been encapsulated within the aqueous interior of lipid vesicles. These range from simple sugars incorporated to enhance image contrast during microscopy to polymers, enzymes, hydrogels, smaller vesicles, or complex collections of molecules such as functional transcription and translation machineries.[2,16−23] With very few exceptions,[18,19,24−28] these encapsulated materials have been uniformly distributed throughout the interior volume of the GVs. In contrast, biological cells display intracellular organization including not only organelles and the cytoskeleton, but also less obvious microcompartments such as multienzyme complexes and heterogeneous local protein concentrations.[29] Intracellular microcompartmentation is dynamic, with changes in local concentrations of various molecules occurring throughout the cell cycle and in response to stimuli.[30−32] For example, the enzymes of the de novo purine biosynthetic pathway colocalized only when purines were not provided in cell growth media,[31] and the assembly of glycolytic enzymes onto erythrocyte membranes is thought to be regulated by phosphorylation and oxygenation.[32] The bacterium *C. crescentus* was recently shown to

Received: March 16, 2011
Published: May 18, 2011

dx.doi.org/10.1021/ja202406v | J. Am. Chem. Soc. 2011, 133, 9545–9555

generate intracellular gradients of protein phosphorylation and consequently DNA replication prior to asymmetric division. The resulting daughter cells differ markedly in morphology and behavior, with one remaining attached to the underlying surface via a stalk and the other using a flagellum to swim away.[33]

Asymmetric division of living cells, in which the resulting daughter cells inherit different biochemical compositions, is crucial for cell differentiation and development in multicellular organisms and also common in unicellular organisms such as yeast and *C. crescentus*.[34−36] Additionally, the asymmetric inheritance of degraded proteins has been implicated in aging,[37] and malfunctions in asymmetric division are thought to play a role in cancer.[35] Mechanisms for asymmetric division in living cells can involve external gradients supplied by the cell's surroundings and/or the asymmetric intracellular distribution of molecules that act as cell fate determinants.[38] A large number of genes have been implicated in generation of biochemical polarity and facilitation of division into nonidentical daughter cells.[38] In addition to the genetic component of cellular asymmetry, a spatial, biophysical component seems likely to serve as the initial cue for the polarity axis.[39] Because newly formed cells arise by division of existing cells, the membrane is inherited from the predivision ("mother") cell, as are the cytoplasm and intracellular contents. An attractive hypothesis is that this inherited material, by providing the cellular architecture in which the genes act, plays a crucial role in the inheritance of polarity. For example, an inherited patch of distinct membrane composition might provide a physical location at which to anchor the cascade of polarity-related molecules and events governed by gene expression in the daughter cells.[39]

We have developed simple model cells that encapsulate a synthetic "cytoplasm" capable of intracellular compartmentation and (bio)chemical polarity.[24,25,27] Our models cells are based on aqueous phase separation in giant lipid vesicles.[26] An aqueous two-phase system (ATPS)[40−43] containing PEG and dextran polymers serves as a primitive model for the cytoplasm, providing macromolecular crowding[44] and distinct microcompartments formed by the two aqueous phases. Differences in local protein concentration can be maintained spatially within individual vesicles by partitioning into the PEG-rich or dextran-rich aqueous phase, and modified by changes in temperature, osmotic pressure, or pH.[24,25,28,40−42] These very simple model cells contain no nucleic acids or enzymes, just this cytoplasm-mimicking polymer solution, the membrane lipids, and some fluorescent proteins added to demonstrate biomolecule compartmentalization. Membrane heterogeneity in the form of coexisting lipid phase domains has been incorporated by using ternary lipid compositions that give rise to liquid disordered (L_d) and liquid ordered (L_o) regions having different lipid composition.[8,45−47]

Herein, we report complete budding and asymmetric fission of these model cells to form nonidentical daughter vesicles that differ in their "cytoplasmic" and membrane compositions, and in some cases are themselves polarized. The ATPS-containing GVs investigated here adopted budded geometries due to osmotic stress, as had been observed previously.[25,27] As external osmolality was increased further, fission of these vesicles occurred, producing nonidentical daughter vesicles. Fission occurred at the aqueous−aqueous phase boundary, resulting in one daughter vesicle that contained the PEG-rich aqueous phase and another that contained the dextran-rich aqueous phase. In some cases, fission was incomplete, with the two daughter vesicles remaining connected by a lipid nanotube; this morphology has been termed "complete budding".[13,45] When coexisting lipid membrane phase domains were also present, these were also inherited unequally, with the PEGylated L_o domain surrounding the PEG-rich aqueous phase, while the L_d domain surrounded the dextran-rich aqueous phase. Fluorescent proteins incorporated in the dextran-rich phase of the aqueous interior and bound to the L_o membrane domain were also asymmetrically inherited by the daughter vesicles. When the available surface area of the L_o and L_d domains did not match the volumes of the PEG-rich and dextran-rich aqueous phases, one of the daughter vesicles inherited both L_o and L_d domains. This daughter could then be exposed to further osmotic stress to generate a second aqueous phase separation and provide asymmetric localization of the newly formed interior aqueous phases.

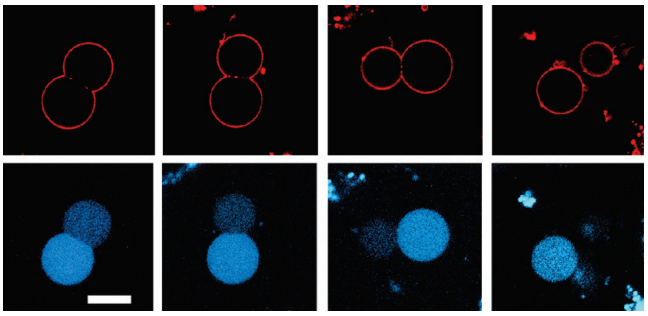

Figure 1. Fission of an ATPS-containing GV in response to osmotic stress. Osmolality increases from left to right. Confocal fluorescence images have been false-colored: red indicates lipid fluorescence (DOPE-rhodamine), and blue indicates Alexa 647-conjugated dextran 10 kDa. The Alexa647 signal decreased over time due to photobleaching; the blue channel has been adjusted to make the partitioning of Alexa 647-conjugated dextran 10 kDa for each time point more apparent. T = 5 °C. Scale bar is 10 μm.

RESULTS AND DISCUSSION

Model cells were prepared by encapsulating a PEG 8 kDa/dextran 10 kDa aqueous two-phase system during formation of giant lipid vesicles by gentle hydration as previously described.[24−28] Briefly, the polymer solution was heated to 42 °C, where it exists as a single phase, during vesicle formation and subsequently cooled to induce phase separation (5 °C). The ATPS-containing giant vesicles were then collected from the bulk ATPS interface and placed in a sucrose solution for observation under the confocal microscope. Because of the preparation protocol, which led to some concentration of the solution due to evaporation, in the work described here most of the vesicles had already adopted a budded morphology prior to observation.[48,49] An example of the budding transition in shown in Supporting Information Figure 1. We will first describe the morphology of model cells with a single-domain membrane composed primarily of DOPC, with 29 mol % cholesterol and small amounts of both DOPE-PEG-2K and DOPE-rhodamine, followed by those with micrometer-scale coexisting L_o and L_d membrane domains. It should be noted that the precise osmolality required to achieve a particular morphology depends on the concentrations of PEG and dextran polymers inside the vesicles in both a straightforward way and also by impacting the composition of each phase and value of the ATPS interfacial tension. Variability in the contents of different individual vesicles within a batch is expected on the basis of our previous studies of polymer encapsulation.[16] We increased the osmolality as needed to force morphological changes

Scheme 1. Asymmetric Fission of Model Cells

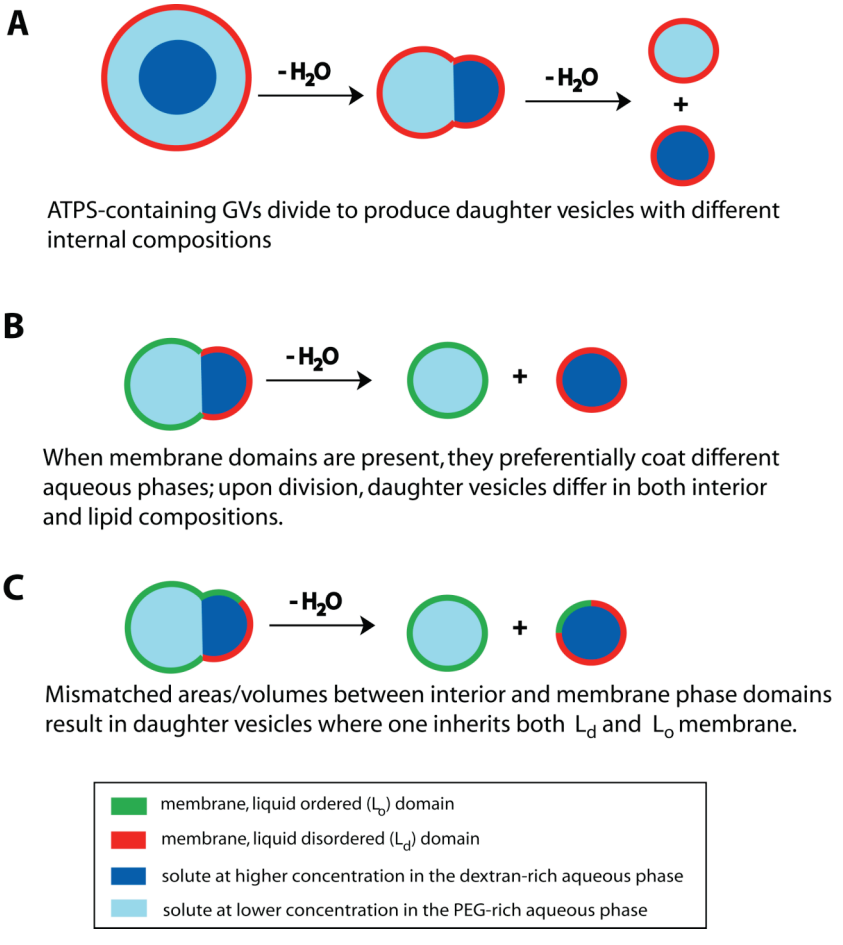

in the ATPS-containing vesicles explored here. A sucrose solution was added every 10−15 min, each time increasing the external concentration by approximately 13% until complete budding or fission occurred. Measurements were performed to determine the osmolality of the starting and ending solutions, which was not additive for these nonideal solutions.

The effect of osmotic stress on a budded, ATPS-containing GV is shown in Figure 1. The initial budded structure had two coexisting aqueous microcompartments corresponding to the two aqueous phases, one enriched in PEG and the other enriched in dextran. The dextran-rich aqueous phase was stained with Alexa 647-labeled dextran 10 kDa for visualization. Addition of sucrose eventually increased the osmolality of the surrounding solution from 122 ± 1.5 to 163 ± 2.6 mmol/kg,[50,52] resulting in the transformation of the initial budded geometry (left) to two spheres connected by a narrow neck (middle panels), and finally to two separate, spherical vesicles that are no longer connected (right). These morphological transformations can be understood in terms of the osmotic pressure difference between the interior and exterior of the vesicles, which resulted in water loss, reducing their volume and concentrating the interior polymer solutions. This provided both excess membrane area over what was required to coat the now smaller volume of the vesicle and increased interfacial tension between the now more concentrated PEG-rich and dextran-rich aqueous phases, driving fission of the mother vesicle.

Fission resulted in chemically distinct daughter vesicles, one containing the dextran-rich aqueous phase and the other containing the PEG-rich aqueous phase of the initial aqueous two-phase system from the mother vesicle (Scheme 1A). The inheritance of distinct aqueous phase volumes provided chemical asymmetry between the daughter cells because the PEG and dextran polymers were present at different concentrations in the two aqueous phases. Partitioning is quantified in terms of the partition coefficient, K, which is the concentration ratio of solute in the PEG-rich phase, C_p, as compared to the dextran-rich phase, C_d, $K = C_p/C_d$. To determine the solute concentration in the aqueous compartments, line scans were performed across both the PEG-rich and the dextran-rich aqueous phases in the GV, and results were compared to calibration curves. For the budded vesicles in Figure 1, $K = 0.60$ for the fluorescent dextran, indicating 1.7× higher concentration in the dextran-rich phase. After fission, the dextran-rich daughter vesicle contained a correspondingly higher concentration of fluorescent dextran than did the PEG-rich daughter vesicle.

Although vesicle fission has been predicted and observed previously in GVs containing homogeneous aqueous interiors,[13,47] the presence of the microcompartmentalized model cytoplasm is an important distinction. Fission of vesicles with simple aqueous interiors has been induced by various external stimuli including laser illumination, heat, changes in phase transitions, and by the addition of phospholipase A_2 and various single-long chain amphiphiles.[10a,11,14,15] For each of these examples, fission was symmetric: each daughter vesicle contained the same interior aqueous solution. In contrast, Figure 1 shows that for ATPS-containing vesicles, fission occurs at the aqueous−aqueous phase

dx.doi.org/10.1021/ja202406v | J. Am. Chem. Soc. 2011, 133, 9545–9555

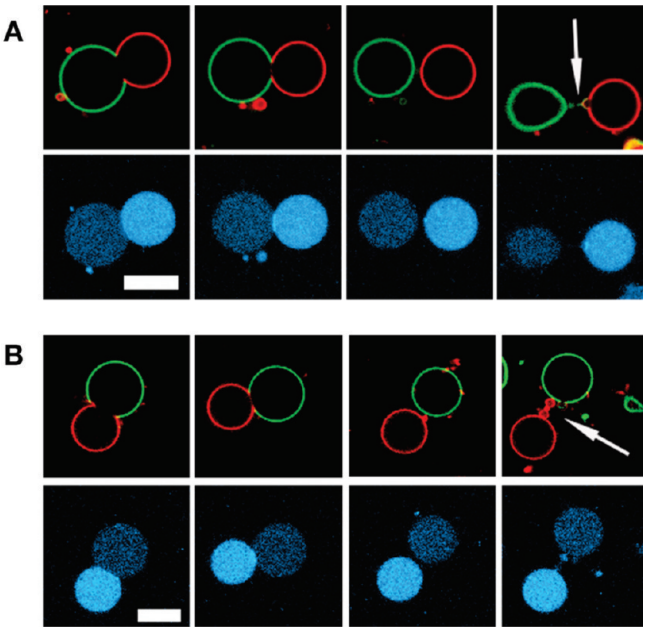

Figure 2. Effect of osmotic stress on two ATPS-containing GVs (A and B) in which lipid membrane phase coexistence was present. The membrane composition for both vesicles was 1:1 DOPC/DPPC + 30% cholesterol, with 2.4% DPPE-PEG-2K, 0.09% DSPE-PEG-2K-biotin, and 0.4% DOPE-rhodamine. Osmolality increases from left to right. Confocal fluorescence images have been overlaid and false-colored: red is DOPE-rhodamine, indicating the L_d membrane domain, and green is streptavidin-Alexa488, bound to DSPE-PEG-2K-biotin, which is partitioned into the L_o membrane domain. Blue indicates lectin SBA-Alexa 647. Arrows on the far right indicate the location of lipid nanotubes between the daughter vesicles. $T = 5$ °C. Scale bars are 10 μm.

boundary such that daughter vesicles have different internal aqueous compositions (Scheme 1A).

Daughter vesicles having different lipid membrane compositions but the same aqueous interior contents have been generated by fission of vesicles with coexisting lipid phase domains (e.g., L_o and L_d). Asymmetric membrane inheritance, where L_d membrane goes to one daughter and L_o to another, occurs when vesicles are exposed to osmotic shock or heated. In these systems, budding and fission are driven by the reduction of line tension at the liquid−liquid phase boundary between the L_o and L_d membrane domains.[13,47] This mechanism fixes the location of fission at the L_o/L_d boundary, such that each daughter vesicle inherits only one lipid phase domain. This can be seen as a two-dimensional membrane analogue of how the three-dimensional aqueous phase domains were split between the daughter vesicles in Figure 1.

We next formed model cells that combined interior aqueous phase separation with membrane L_o/L_d phase separation. This was accomplished by incorporating a ternary lipid composition selected to provide lateral phase separation based on the phase diagrams from the Keller lab,[7,46] with a few modifications to adapt it for use in our work. Specifically, lipids having PEGylated headgroups were added to provide preferential wetting of the PEG-rich aqueous interior phase with a PEGylated L_o membrane domain; this preferential wetting and the altered temperature-dependence of L_o/L_d phase separation in our ternary lipid mixture have been explored in a previous publication.[27] Here, we also incorporated greater biomolecular complexity in these model cells by adding fluorescently labeled proteins to the interior and exterior of the vesicles. Soybean agglutinin (SBA) labeled with Alexa647 was added to the ATPS; this protein partitions into the dextran-rich aqueous compartment. A small amount of biotinylated lipid, DSPE-PEG-2K-biotin, which partitions into the L_o membrane phase domain, was added during vesicle formation. Streptavidin labeled with Alexa488 was added after vesicle budding to stain the L_o domain (Supporting Information Figure 2). Figure 2 (leftmost panels) shows the distribution of these molecules in the budded model cells. The SBA was found as anticipated in the aqueous phase wetted by the L_d membrane; this is consistent with the dextran-rich phase based on known partitioning of SBA in PEG/dextran ATPS[24,25] and with our previous work with L_o and L_d membranes wetting PEG/dextran ATPS.[27] For the initial vesicles in Figure 2A and B (left), the local lectin concentration was ∼4× higher in the dextran-rich phase as compared to the PEG-rich aqueous phase (e.g., for the vesicle in Figure 2A, $C_p = 64 \pm 5$ nM, $C_d = 264 \pm 13$ nM).

Approximately every 15 min after initial image acquisition, sucrose was added to increase the osmotic pressure of the external solution, from 122 ± 1.5 mmol/kg initially to 142 ± 1.5 mmol/kg for the vesicle shown in Figure 2A. As was observed for the single-phase membranes shown in Figure 1, separation into two spherical or quasispherical daughters occurred in response to the osmotic stress. Here, the dextran-rich daughter vesicles contained higher internal protein (SBA) concentrations and were surrounded by L_d membrane, and the PEG-rich daughter vesicles were in contact with the L_o membrane, on which the membrane-bound protein (streptavidin) was localized. Thus, separation resulted in asymmetric inheritance of both the interior composition, including a soluble protein, and the membrane lipids with their associated protein. For example, in Figure 2A, the concentration of "cytoplasmic" protein was 5-fold higher in the dextran-rich daughter vesicle as compared to the PEG-rich daughter vesicle ($K = 0.19 \pm 0.02$). Fluorescence signal from the labeled streptavidin was only associated with the L_o phase domain, and hence a partitioning coefficient for this protein in the membrane cannot be calculated; it appears to have been inherited exclusively by the PEG-rich daughter vesicles. Similar results were obtained for the vesicle in Figure 2B, for which osmolality was increased from 108 ± 2.6 mmol/kg initially to 216 ± 6.5 mmol/kg in the panel to the far right. Because of differences in vesicle volume vesicle-to-vesicle variability in the internal concentrations of PEG and dextran polymers,[16] the external osmolality required to induce these morphological changes was not identical for all vesicles.

In some cases, a lipid nanotube could be seen connecting the daughter vesicles (see arrows in far right panels, Figure 2A and B). Such structures are not uncommon in the vesicle literature; when a force is applied to a vesicle, the membrane can deform to produce lipid tubes (tethers), as a way to protect the integrity of the membrane.[5,54] Complete budding is distinct from fission in the presence of a shared lipid nanotube and its aqueous contents.[13,45] Membrane tethers have been produced by means of hydrodynamic flow, micropipets, optical tweezers, and kinesein motor proteins.[55−60] Li et al. recently reported the generation of many lipid nanotubes *inside* ATPS-containing giant vesicles in response to osmotic stress.[61] There, nanotubes accumulated at the aqueous/aqueous interface and in effect served as a storage site for excess membrane area, which could be pulled back into the main membrane by increasing membrane tension.[61] We presume that nanotube formation similarly occurred here as a result of excess

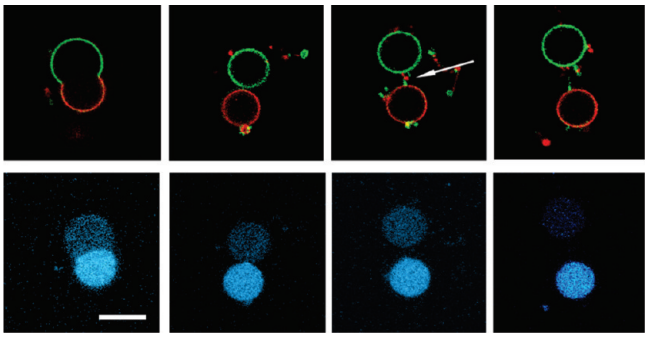

Figure 3. Confocal fluorescence images collected during asymmetric division of ATPS-containing GV presenting micrometer-scale lipid domains (lipid composition was 1:1 DOPC/DPPC + 30% cholesterol, with 2.2% DPPE-PEG-2K, 0.08% DSPE-PEG2K-carboxyfluorescein, and 0.08% DOPE-rhodamine). Osmolality increases from left to right (130 ± 1.5 mmol/kg to 238 ± 5.5 mmol/kg). Fluorescence images have been false colored: red indicates DOPE-rhodamine in the L_d membrane domain, and green indicates DSPE-PEG 2000-carboxyfluorescein, in the L_o membrane domain, and blue indicates Alexa 647-lectin SBA. The Alexa647 signal decreased over time due to photobleaching; the blue channel has been adjusted to make the partitioning of SBA apparent for each time point. T = 5 °C. Scale bar is 10 μm.

membrane area upon volume loss, and the accumulation of this lipid material at the aqueous/aqueous phase boundary may have facilitated both the fission and/or complete budding transitions and the formation of nanotube tethers that often connected the daughter vesicles. For the two vesicles shown in Figure 2, the connecting nanotubes did not break even at the highest osmolalities tested (142 ± 1.5 mmol/kg for Figure 2A, and 216 ± 6.5 mmol/kg for Figure 2B).

Coexisting L_o and L_d domains can facilitate fission of tubes pulled from GVs.[62,63] For example, Allain et al. demonstrated that breakage, or fission, occurred in membrane nanotubes with coexisting L_o/L_d domains and was not observed in homogeneous lipid membrane tethers.[62] For the vesicles in Figure 2, the nanotubes appear to be a single phase. The daughter vesicles in Figure 2 A are connected by a nanotube composed of lipid in the L_o phase (see also Supporting Information Figure 3), while the nanotube in Figure 2B appears to be entirely composed of L_d lipids. The nanotube in Figure 2B appears to display pearling; pearling instabilities have been reported when tubular structures were destabilized by optical tweezers,[64] induced curvature,[65] anchored polymer,[66] and nanoparticle binding[67] and observed in axons in which pearling was driven by osmotic perturbations.[68]

It should be noted that streptavidin binding has also been shown to cause nanotube formation.[69] Protein−membrane interactions can alter the membrane's curvature through anchor insertion[70] and can induce nanotube formation through a number of ways including the protein's structure,[71] through protein assemblies,[72,73] and by altering the surface charge of the membrane.[74] It is not difficult to imagine that the deformation of the membrane and production of tubular structures, via streptavidin binding, may participate in the morphological changes observed in our system. However, streptavidin was not required for fission (see Figure 1), and nanotube formation still occurred in the absence of streptavidin. For example, Figure 3 shows a model cell with no protein bound to its membrane, which still divided asymmetrically to produce daughter vesicles originally connected by a membrane tether, which then ruptured.

For the vesicle in Figure 3, we used fluorescently labeled lipid, DSPE-PEG 2000-carboxyfluorescein, in place of DSPE-PEG 2000-biotin−streptavidin-AF488, for tracking of the L_o phase. As before, the PEG-rich bud was initially surrounded by the PEGylated L_o membrane, and the dextran-rich bud was in contact with the L_d phase. Osmotically driven asymmetric fission resulted in separate daughter vesicles: a PEG-rich daughter vesicle with L_o membrane, and a dextran-rich daughter surrounded by L_d membrane. Similar to the fission events in Figure 2, there was a 4-fold difference in local lectin concentration in the dextran-rich daughter vesicle as compared to the PEG-rich daughter vesicle (C_p = 18 ± 4 nM, C_d = 71 ± 12 nM). A membrane tether of primarily L_o lipid (green), with some L_d (red), initially connected the two daughter vesicles (third panels from right), but ultimately broke to release the daughter vesicles (last panels). To verify that the nanotube connecting the daughter vesicles had indeed broken rather than simply moved out of the focal plane, we added water to the external solution to reduce osmolality and induce vesicle swelling. Rather than a reversal of the fission event, we observed an increase in the distance between the PEG-rich and dextran-rich daughter vesicles until they were no longer visible in the same focal plane. Dilutions performed for other daughter vesicles usually yielded similar results: addition of water led to nanotube breakage due to fluid flow, facilitating the completion of the vesicle fission events rather than reversing them. Fusion of the daughter vesicles and retraction of the bud to form a single, spherical vesicle was never observed; however, in some cases the nanotubes persisted rather than breaking. Vesicles connected by a nanotube ruptured approximately 50% of the time. Breakage of the membrane tether was usually observed as a result of fluid flow from the addition of sucrose or deionized water to the external solution, including collisions with other vesicles in the suspension due to this flow.

In Figures 2 and 3, and for the majority of vesicles we observed for these membrane compositions, each daughter vesicle inherited only L_o or L_d phase lipid compositions, that is, only green or red membrane (Scheme 1B). This is similar to what has been observed for daughter vesicles generated by line tension-driven fission of GVs that lack an ATPS and suggested that line tension at the L_o/L_d phase boundary was important in our system despite the fact that it was not required for achieving fission (see Figure 1). Our ATPS-containing vesicles also have an interfacial tension at the boundary between the PEG-rich and dextran-rich aqueous phases. Interfacial tensions for PEG/dextran ATPS are on the order of 5×10^{-3} dyn/cm for the composition initially encapsulated and can be expected to increase by 1 or more orders of magnitude with the increased total polymer concentration that occurs when vesicle volume is osmotically decreased by as much as half.[25,75]

When the mole ratio of DOPC to DPPC was 1:1, the relative surface areas of the L_o and L_d phases were approximately equal and matched the relative volumes of the interior aqueous phases. This can be seen in the budded ATPS GVs (Figures 2 and 3), in which the L_o/L_d phase boundary coincides with the PEG/dextran interface. Upon division, the PEG-rich daughter vesicle is surrounded entirely by L_o phase, and the dextran-rich daughter vesicle only contains membrane in the L_d phase. However, phase boundary mismatch had been observed in ATPS-containing GVs for which the relative phase volumes were ~2:1, resulting in more L_d phase than required to coat the dextran-rich bud, and thus partial contact of the L_d phase with the PEG-rich bud.[27] We therefore prepared model cells in which L_o and L_d membrane areas were mismatched with respect to the interior aqueous

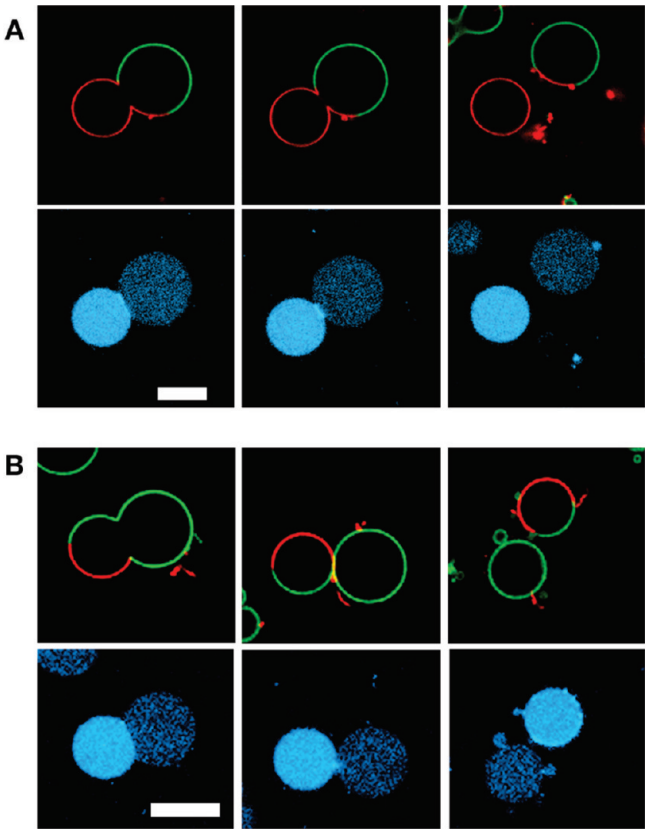

Figure 4. Division of ATPS-containing GVs with excess area of either L_d or L_o membrane domain. Membrane compositions were as follows: 1:1 DOPC/DPPC + 30% cholesterol (A), 1:2 DOPC/DPPC + 30% cholesterol (B). Osmolality increases from left to right. Fluorescence images have been overlaid and false-colored. Blue indicates lectin SBA-Alexa 647, red indicates L_d domain lipid (DOPE-rhodamine), and green indicates L_o domain streptavidin-Alexa488 (bound to lipid DSPE-PEG-2K-biotin). T = 5 °C. Scale bar is 10 μm.

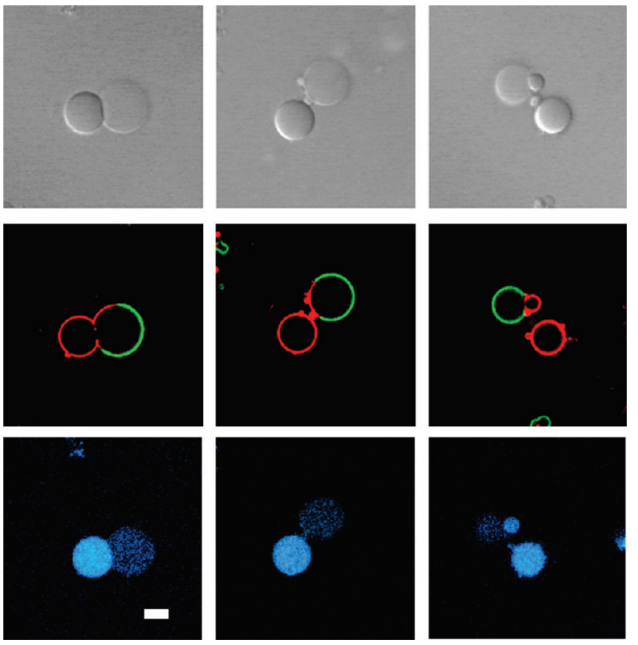

Figure 5. Second-generation aqueous phase separation and budding in a daughter vesicle. Membrane composition was 1:2 DOPC/DPPC + 30% cholesterol. Osmolality increases from left to right. Panels top to bottom are transmitted light (DIC), membrane fluorescence, and interior protein fluorescence. Confocal fluorescence images have been overlaid and false-colored. Red indicates L_d domain lipid (DOPE-rhodamine), green indicates L_o domain lipid (streptavidin-Alexa 488, bound to DSPE-PEG 2000-biotin), and blue indicates the lectin, SBA-Alexa 647, which is partitioned into the dextran-rich interior aqueous phase. T = 5 °C. Scale bar is 10 μm.

phase volumes to examine the consequences of membrane/interior phase mismatch on fission.

Figure 4 shows how a mismatch in membrane domain area and interior aqueous phase volume results in inheritance of both L_o and L_d membrane domains by one of the two daughter vesicles (Scheme 1C). The left-hand panels of Figure 4 A and B show budded vesicles in which the interface of the L_o/L_d domains does not coincide with the interior aqueous−aqueous phase boundary. In Figure 4A (left), the surface area of the interior dextran-rich bud was smaller than the available L_d membrane area, such that the L_d membrane also coats part of the PEG-rich aqueous phase. The opposite situation is observed in Figure 4B (left), with part of the L_o lipid phase domain coating the dextran-rich aqueous phase bud. Addition of sucrose to the external solution resulted in invagination of the membrane at the aqueous−aqueous interface between the PEG-rich and dextran-rich phases (middle). A further increase in external osmolality resulted in complete budding and/or fission (far right panels). Here, one of the two daughter vesicles inherited the larger-area membrane domain, and the other inherited both L_o and L_d membrane domains. Which daughter ended up with the dual-phase membrane depended on the initial mismatch of internal aqueous volumes and membrane domain surface areas. This was controlled by varying the ATPS composition to achieve different relative volumes of the PEG-rich and dextran-rich phases or by varying the lipid composition to achieve different relative areas of L_o and L_d membrane domains. For example, the ratio of DOPC to DPPC ratio was increased to 1:2 for the vesicle shown in Figure 4B. Additional examples, in which 1:1.5 DOPC/DPPC + 30% cholesterol were used, are shown in Supporting Information Figure 4. These data indicate the primacy of the aqueous−aqueous phase boundary in determining the site of vesicle division: division always occurred at the aqueous−aqueous phase boundary but only sometimes at the L_o/L_d phase boundary. The resulting daughter vesicles each contained one of the two aqueous phase volumes in its entirety and were coated by whatever membrane composition was necessary to enable this. As for the 1:1 lipid composition used above, when these 1:2 and 1:1.5 DOPC:DPPC lipid ratio vesicles formed daughter vesicles connected by a nanotube after osmotic stress, they subsequently lost this connection, converting to full fission events, approximately one-half of the time. We note that in some cases, even nanotubes that appeared to contain only the L_d lipid domain ruptured during the course of our experiments. Whether a given nanotube remained or ruptured when water was added in an attempt to reverse the budding event appeared to depend more on forces exerted on the structures by fluid flow than on their L_o/L_d composition.

The ability to produce daughter vesicles in which membrane asymmetry is inherited from the mother vesicle is interesting as a primitive model of polarity inheritance in biological cells. An important question in cell biology is how polarity cues are inherited during cell division. In addition to genetic inheritance, membrane type and polarity are also continuous through

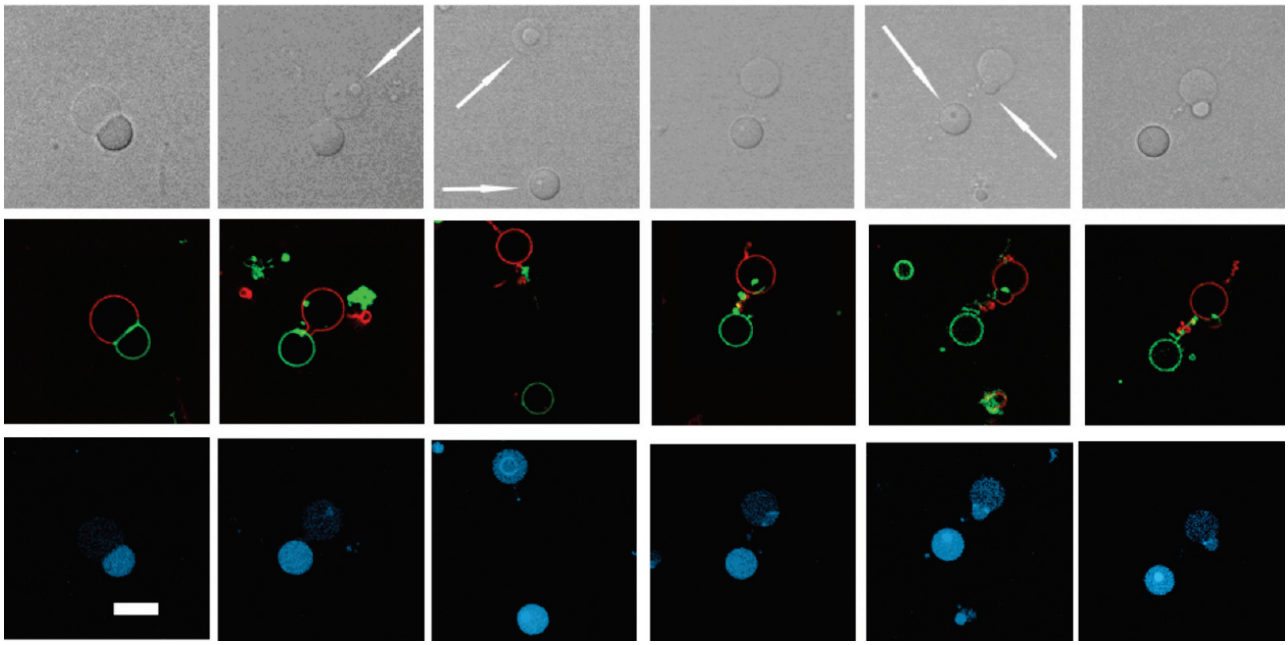

Figure 6. Aqueous phase separation in each of resulting vesicles after complete budding to form two daughter vesicles connected by a lipid nanotube. Membrane composition was 1:1 DOPC/DPPC + 30% cholesterol. Osmolality increases from left to right. Top row is transmitted light (DIC). Fluorescence images have been overlaid and false-colored. Green indicates L_d domain lipid (DOPE-CF), red indicates L_o domain (streptavidin-Cy3, bound to lipid DSPE-PEG 2000-biotin), and blue indicates lectin SBA-Alexa 647 (note that the red and green dyes are reversed as compared to previous figures). Arrows highlight the location of newly formed aqueous phases within each of the daughter vesicles. T = 5 °C for the first three panels and 32 °C for the last three panels. Scale bar is 10 μm.

generations.[39,76] One hypothesis suggests that the membrane, which is passed on directly from the mother cell, may play an important role in polarity initiation in daughter cells, serving as a landmark for localization of a cascade of biochemical events that generate polarity in the daughter cells.[39,76] Such a cascade could occur, for example, by a patch of membrane recruiting molecules from the cell interior to form a microdomain on or near that membrane patch to initiate the polarity cascade by providing spatial organization to the many gene products known to be involved in polarity.

We observed several instances in which an inherited patch of L_o or L_d membrane in one of the daughter vesicles formed a bud due to additional phase separation of the encapsulated aqueous volume under osmotic stress. This process led to polarity in the membrane, the aqueous interior, and the distribution of internal and external proteins (i.e., SBA, which was partitioned into the dextran-rich aqueous phase, and streptavidin, which was bound to the biotinyated L_o membrane domain). An example is shown in Figure 5. Initially in a 122 ± 1.5 mmol/kg solution, the L_d phase of the mother vesicle is contacting the PEG-rich bud (top panel). Fission, which was associated with an approximately 20−25% further loss in volume at a final osmolality of 157 ± 8.5 mmol/kg solution, resulted in daughter vesicles connected by a membrane tether (middle panel). The PEG-rich daughter vesicle inherits both the L_o domain, on which the streptavidin-AF488 is localized, and a portion of the L_d domain, which was present in excess over what was required to coat the dextran-rich daughter vesicle. Inside the vesicles, the PEG-rich daughter vesicle contained approximately 3.5× less protein (12 nM) than the dextran-rich daughter vesicle, which had 43 nM SBA. Further exposure to osmotic stress caused the PEG-rich daughter vesicle to bud (right-hand panel). This was possible because the PEG-rich aqueous phase contains both PEG and dextran polymers, which upon concentration due to osmotic dehydration formed a new aqueous two-phase system, albeit with a smaller volume dextran-rich phase than in the original mother vesicle. This is apparent in the transmitted light (DIC) image, as well as in the blue channel showing the location of SBA, which has partitioned into the new dextran-rich phase bud, with a 2-fold difference in local "cytoplasmic" protein concentration between the bud and body of the vesicle (C_d = 27 nM, C_p = 12 nM; K = 0.42).

Phase separation in what was formerly the PEG-rich phase of the ATPS can be understood in the context of the compositions of the two phases. On the basis of partitioning measurements, the PEG-rich phase of an encapsulated ATPS with an intended composition 7 wt % PEG 8 kDa and 10 wt % dextran 10 kDa contains on the order of 2× as much PEG and 0.5× as much dextran as the dextran-rich phase.[24] In general, significant concentrations of both polymers are present in each phase of an ATPS, with the relative concentrations and relative volumes determined by the ATPS composition relative to the binodal and tie lines.[40,43] The composition of each phase lies on the binodal curve that separates single-phase solutions from two-phase coexistence. Hence, in our system, once the two phases are split from each other by vesicle fission, any further increase in polymer concentration due to volume loss can cause the individual solutions to phase separate within the daughter vesicles. In some cases, we observed phase separation in both the PEG-rich and the dextran-rich daughter vesicles. An example is shown in Figure 6.[77] This vesicle was exposed to a higher external sucrose concentration than those discussed above (osmolality was increased to 452 ± 0.5 mmol/kg).

Phase separation in the PEG-rich daughter vesicle is apparent in the second panel of Figure 6, with the tiny dextran-rich phase first appearing as a droplet fully surrounded by the PEG-rich phase in the second panel. Phase separation in the dextran-rich

daughter vesicle can be seen in the third panel, with the tiny new phase surrounded by the larger phase. At this point, deionized water was added to test whether the daughter vesicles were still attached by a nanotube; they were still attached and moved closer together in response to this decrease in external osmolality. The sample was also heated from 5 to 32 °C between panels 3 and 4 of Figure 6; heating did not result in breakage of the nanotube but did facilitate budding of the newly formed dextran-rich aqueous phase from the PEG-rich daughter vesicle (fifth and sixth panels).

Fluorescence from the SBA was concentrated into the smaller phase volume of both daughter vesicles, which was unexpected because the smaller phase within the dextran-rich daughter should be the newly formed PEG-rich phase.[40,43] The transmitted light DIC images for this vesicle also suggested to us that the smaller phase was indeed the PEG-rich phase,[27] contrary to the expected (and routinely observed) partitioning of this protein into the dextran-rich phase. These data indicate that the high local concentration of SBA in the dextran-rich daughter vesicle, coupled with macromolecular crowding from the polymers, may have caused protein aggregation that resulted in accumulation of the SBA either in the PEG-rich phase or at the aqueous−aqueous interface in this daughter vesicle. We have previously observed both accumulation of protein aggregates at the aqueous−aqueous phase boundary and partitioning of denatured proteins into the PEG-rich phase of GV-encapsulated ATPS.[28] SBA can also be seen accumulating at the aqueous/aqueous interface of the L_d daughter vesicle (shown in red) after phase separation (third panel). For the vesicles shown in Figures 5 and 6, the occurrence of a second phase separation event in the daughter vesicles was possible only after they had become separate structures; when PEG-rich and dextran-rich phases are in the same container, a loss of volume results in a change in the composition of the phases but does not generate additional phases. Although the nanotube in Figure 6 persisted even after dilution and heating, the two aqueous volumes do not appear to be in communication on the time scale of these experiments (tens of minutes).

CONCLUSIONS

Polarized "mother" vesicles divided to produce chemically distinct daughter vesicles, each inheriting different membrane and interior compositions as well as different concentrations of soluble and membrane-bound proteins. This was possible by taking advantage of an aqueous two-phase system as a model cytoplasm that provided several important features: macromolecular crowding, protein sorting via partitioning between the aqueous phases, "pinning" the location of the PEGylated L_o membrane to the PEG-rich aqueous phase, and fixing the location for the division plane. Although biological cells do not contain simple ATPS, the cytoplasm of living cells is compartmentalized, allowing for differences in local concentration. Aqueous phase separation is biophysically reasonable in the macromolecularly crowded intracellular milieu and has in rare cases been observed in living cells.[78−80] Likewise, biological membranes are known to exhibit spatial heterogeneity,[81] which was modeled here by simple liquid phase coexistence. Although multiple divisions were precluded here by the limited amount of membrane area available, self-replicating vesicles have been reported based on, for example, addition of surfactant or fatty acid precursors to existing fatty acid or lipid vesicles.[82,83] Retention of encapsulated molecules through multiple cycles of growth and reproduction has been reported.[84] It may ultimately be possible to couple such an approach with the compartmentalized membranes and interiors used here to produce additional "generations" of asymmetrically dividing vesicles. We have introduced a simple, nonliving experimental model system for asymmetric fission, which underscores the apparent complexity of behaviors that can result from simple chemical and physical interactions such as self-assembly, phase separation, and partitioning. Additionally, this work supports the possibility that spatial/organizational cues, in addition to genetic signals, could be important for achieving and maintaining polarity through cell division cycles.

EXPERIMENTAL METHODS

Chemicals and Materials. 1,2-Dioleoyl-*sn*-glycero-3-phosphocholine (DOPC), 1,2-dipalmitoyl-*sn*-glycero-3-phosphocholine (DPPC), dipalmitoyl-*sn*-glycero-3-phosphoethanolamine-*N*-[methoxy(polyethylene glycol)-2000] (DPPE-PEG 2000), 1,2-distearoyl-*sn*-glycero-phosphoethanolamine-*N*-[biotinyl(polyethylene glycol)2000] (DSPE-PEG 2000-biotin), 1,2-distearoyl-*sn*-glycero-3-phosphoethanolamine-*N*-[poly(ethyleneglycol) 2000-*N*′-carboxyfluorescein] (DSPE-PEG 2000-FITC), 1,2-dioleoyl-*sn*-glycero-3-phosphoethanolamine-*N*-(lissamine rhodamine B sulfonyl) (DOPE-rhodamine), 1,2-dioleoyl-*sn*-glycero-3-phosphoethanolamine-*N*-(carboxyfluorescein), and 1,2-dioleoyl-*sn*-glycero-3-phosphoethanolamine-*N*-[methoxy(polyethylene glycol)-2000] were purchased as chloroform solutions from Avanti Polar Lipids, Inc. (Alabaster, AL). Cholesterol was from Supelco (Bellefonte, PA). The polymers, poly(ethylene glycol) (PEG) 8 kDa, dextran 10 kDa, and sucrose, were purchased from Sigma Chemical Co. (St. Louis, MO). Alexa Fluor 647-conjugated lectin SBA, Alexa488-labeled streptavidin, Alexa 647-conjugated dextran 10 kDa, and the press-to-seal silicone spacers were from Invitrogen (Eugene, OR). Water used in these experiments was purified to a resistivity of ≥18.2 MΩ with a Barnstead NANOPure Diamond system from Barnstead International (Dubuque, IA).

Preparation of Giant Vesicles with Coexisting Fluid Phases Encapsulating an Aqueous Two-Phase System. Lipid vesicles were formed using the gentle hydration method, as previously described,[85] with slight modifications.[24,25,27] Briefly, a 1:1 molar ratio of DOPC/DPPC + 30% cholesterol was prepared by the addition of 34% DOPC, 34% DPPC, 30% cholesterol, 2.0% DPPE-PEG 2000, 0.09% DOPE-rhodamine, and 0.08% DSPE-PEG2000-biotin to a test tube (10 × 75 mm, Durex borosilicate glass, VWR, Int., West Chester, PA) containing ∼100 μL of chloroform. The lipid solution was then dried under Ar (g) to produce a thin, lipid film. Residuals of chloroform were removed by placing the test tube under vacuum desiccation for approximately 2 h. During this time, a bulk ATPS solution consisting of 7 wt % PEG 8 kDa and 10 wt % dextran 10 kDa in water was prepared and incubated at 43 °C (Supporting Information Figure 5 shows the phase diagram and the temperature-dependence of phase separation in this system). Next, 990 μL of warm, single-phase polymer solution and 10 μL of Alexa Fluor 647-lectin SBA (2 mg/mL) were added along the wall of the test tube, and the lipids were hydrated at 43 °C for approximately 48 h. The same procedure was followed for the preparation of GVs with ratios of 1:1.5 (22.7 mol % DOPC, 45.5 mol % DPPC) and 1:2 DOPC/DPPC + 30% cholesterol (27.2 mol % DOPC, 40.7 mol % DPPC).

Preparation of ATPS/GV Samples for Confocal Microscopy. After vesicle formation at 43 °C, sample vials were transferred to 5 °C, a temperature below the ATPS transition, to drive phase separation both in the bulk solution and in the vesicle interior. Vesicles accumulated at the interface of the phase-separated bulk ATPS, from which 1−2 μL of vesicles was removed and transferred to a shallow well made from placing a silicone spacer on a microscope coverslip (24 × 60 mm, VWR Int., West Chester, PA). Vesicles were first diluted with 10 μL of 5 °C PEG-rich top phase, and then an aliquot (10−30 μL) of 130 mM sucrose and 0.5 μL of Alexa 488-streptavidin (9.25 μM) were added to the sample solution. An Anodisc 25 membrane (0.2 μm diameter pores) (Whatman International Ltd., Maidstone, England) was

placed on top of the press-to-seal silicon spacer to facilitate addition of further aliquots of sucrose solution with minimal disturbance of the vesicles under observation (when solution is pipetted directly in rather than through the membrane, flow often results in loss of the vesicles from the field of view). A sucrose solution was added every 10−15 min, each time increasing the external solution concentration by approximately 13%, until fission occurred. The 10−15 min delay provided sufficient time for morphological changes; no further changes occurred after 15 min unless additional changes in osmolality were provided. The amount of sucrose needed to achieve fission varied from vesicle to vesicle due to variability in the PEG and dextran encapsulation[16] and in vesicle volume.

Quantification of Protein Partitioning in ATPS-Containing Vesicles. Protein (Alexa Fluor 647-lectin SBA) and polymer concentrations (Alexa Fluor 647-dextran 10 kDa) in the PEG-rich and dextran-rich phases were determined from their fluorescence intensities by taking a line scan across the PEG-rich and dextran-rich compartments in the vesicle. Solute concentrations were determined directly from the confocal fluorescence intensities using a calibration curve of the labeled protein at different concentrations also acquired on the confocal microscope under identical imaging conditions. Partitioning was calculated as the partition coefficient, K, defined as $K = C_p/C_d$, where C_p is the concentration of the solute in the PEG-rich phase and C_d is its concentration in the dextran-rich phase.

Instrumentation and Software. ATPS GV confocal images were acquired using an Olympus IX-70 laser scanning confocal inverted microscope (LSCM) (Nikon Plan Apo 60× 1.4 NA objective) or an LSM-5 Pascal laser scanning confocal microscope from Carl Zeiss, Inc. (Oberkochen, Germany) with a Plan-Apochromat 63× oil immersion objective (1.4 NA) and Pascal Software as previously described.[25,27] A temperature-controlled PE-100 microscope stage, a PE-94 control unit (both from Linkam, ±0.1 °C), and a circulating water bath from VWR (model 1160A) were used to control GV suspension temperature. A microprobe (model IT-21) from Harvard apparatus and a Physitemp-BAT-12 readout unit (±0.1 °C) were used to directly measure GV suspension temperature. A VAPRO vapor pressure osmometer (model 5500) from Wescor, Inc., was used to measure solution osmolality at 25 °C.

■ ASSOCIATED CONTENT

Supporting Information. Confocal optical microscope images showing ATPS-containing vesicles pre- and post-budding, before and after external Alexa 488-streptavidin addition, additional fission examples, and a phase diagram for the PEG 8 kDa/dextran 10 kDa ATPS at 5 and 37 °C. This material is available free of charge via the Internet at http://pubs.acs.org.

■ AUTHOR INFORMATION

Corresponding Author
keating@chem.psu.edu

■ ACKNOWLEDGMENT

This work was primarily supported by the National Science Foundation, Grant CHE-0750196, cofunded by the MCB division, with additional support from the National Institutes of Health, Grant R01GM078352. We thank Owe Orwar for helpful discussions and suggesting that we look for nanotubes in these dividing vesicles. Some of the confocal microscopy images were obtained at the Center for Quantitative Cell Analysis, a shared facility of The Huck Institutes of the Life Sciences at The Pennsylvania State University.

■ REFERENCES

(1) (a) Menger, F. M.; Gabrielson, K. D. *Angew. Chem., Int. Ed. Engl.* **1995**, *34*, 2091–2106. (b) Menger, F. M.; Angelova, M. I. *Acc. Chem. Res.* **1998**, *31*, 789–797. (c) Oberholzer, T.; Luisi, P. L. *J. Biol. Phys.* **2002**, *28*, 733–744.(d) *Liposomes: A Practical Approach*, 2nd ed.; Torchilin, V. P., Weissig,V., Eds.; Oxford University Press: Oxford, 1990.

(2) *Giant Vesicles, Perspectives in Supramolecular Chemistry 6*; Luisi, P. L., Walde, Eds.; John Wiley and Sons: West Sussex, 2000.

(3) Walde, P.; Cosentino, K.; Engel, H.; Stano, P. *ChemBioChem* **2010**, *11*, 848–865.

(4) Jesorka, A.; Orwar, O. *Annu. Rev. Anal. Chem.* **2008**, *1*, 801–832.

(5) Dimova, R.; Aranda, S.; Bezlyepkina, N.; Nikolov, V.; Riske, K. A.; Lipowsky, R. *J. Phys.: Condens. Matter* **2006**, *18*, S1151–S1176.

(6) Rawicz, W.; Smith, B. A.; McIntosh, T. J.; Simon, S. A.; Evans, E. *Biophys. J.* **2008**, *94*, 4725–4736.

(7) Veatch, S. L.; Keller, S. L. *Biochim. Biophys. Acta* **2005**, *1746*, 172–185.

(8) Svetina, S. *ChemPhysChem* **2009**, *10*, 2769–2776.

(9) (a) Menger, F. M.; Lee, S. J. *Langmuir* **1995**, *11*, 3685–3689. (b) Hatta, E. *J. Phys. Chem. B* **2007**, *111*, 10155–10159.

(10) (a) Döbereiner, H.-G.; Käs, J.; Noppl, D.; Sprenger, I.; Sackmann, E. *Biophys. J.* **1993**, *65*, 1396–1403. (b) Yu, Y.; Vroman, J. A.; Bae, S. C.; Granick, S. *J. Am. Chem. Soc.* **2010**, *132*, 195–201.

(11) (a) Staneva, G.; Angelova, M. I.; Koumanov, K. *Chem. Phys. Lipids* **2004**, *129*, 53–62. (b) Staneva, G.; Seigneuret, M.; Koumanov, K.; Trugnan, G.; Angelova, M. I. *Chem. Phys. Lipids* **2005**, *136*, 55–66.

(12) Seifert, U.; Berndl, K.; Lipowsky, R. *Phys. Rev. A* **1991**, *44*, 1182–1202.

(13) (a) Jülicher, F.; Lipowsky, R. *Phys. Rev. E* **1996**, *53*, 2670–2683. (b) Lipowsky, R. *Biophys. J.* **1993**, *64*, 1133–1138. (c) Lipowsky, R.; Dimova, R. *J . Phys.: Condens. Matter* **2003**, *15*, S31–S45. (d) Lipowsky, R. *J. Phys. II France* **1992**, *2*, 1825–1840.

(14) (a) Leirer, C.; Wunderlich, B.; Myles, V. M.; Schneider, M. F. *Biophys. J.* **2009**, *143*, 106–109. (b) Kitamura, N.; Sekiguchi, N.; Kim, H.-B. *J. Am. Chem. Soc.* **1998**, *120*, 1942–1943.

(15) (a) Inaoka, Y.; Yamazaki, M. *Langmuir* **2007**, *23*, 720–728. (b) Tanaka, T.; Sano, R.; Yamashita, Y.; Yamazaki, M. *Langmuir* **2004**, *20*, 9526–9534.

(16) (a) Dominak, L. M.; Keating, C. D. *Langmuir* **2007**, *23*, 7148–7154. (b) Dominak, L. M.; Keating, C. D. *Langmuir* **2008**, *24*, 13565–13571. (c) Dominak, L. M.; Omiatek, D. M.; Gundermann, E. L.; Heien, M. L.; Keating, C. D. *Langmuir* **2010**, *26*, 13195–13200.

(17) Walde, P.; Ichikawa, S. *Biomol. Eng.* **2001**, *18*, 143–177.

(18) (a) Jesorka, A.; Markström, M.; Orwar, O. *Langmuir* **2005**, *21*, 1230–1237. (b) Markström, M.; Gunnarsson, A.; Orwar, O.; Jesorka, A. *Soft Matter* **2007**, *3*, 587–595. (c) Viallat, A.; Dalous, J.; Abkarian, M. *Biophys. J.* **2004**, *86*, 2179–2187. (d) Kiser, P. F.; Wilson, G.; Needham, D. *Nature* **1998**, *394*, 459–462.

(19) (a) Kusumaatmaja, H.; Li, Y.-H.; Dimova, R.; Lipowsky, R. *Phys. Rev. Lett.* **2009**, *103*, 238103–1−4. (b) Li., Y.-H.; Lipowsky, R.; Dimova, R. *J. Am. Chem. Soc.* **2008**, *130*, 12252–12253.

(20) Bolinger, P.-Y.; Stamou, D.; Vogel, H. *J. Am. Chem. Soc.* **2004**, *126*, 8594–8595.

(21) Noireaux, V.; Libchaber, A. *Proc. Natl. Acad. Sci. U.S.A.* **2004**, *101*, 17669–17674.

(22) (a) Kuruma, Y.; Stano, P.; Ueda, T.; Luisi, P. L. *Biochim. Biophys. Acta* **2009**, *1788*, 567–574. (b) Chiarabelli, C.; Stano, P.; Luisi, P. L. *Curr. Opin. Biotechnol.* **2009**, *20*, 492–497.

(23) (a) Yu, W.; Sato, K.; Wakabayashi, M.; Nakaishi, T.; Ko-Mitamura, E. P; Shima, Y.; Urabe, I.; Yomo, T. *J. Biosci. Bioeng.* **2001**, *92*, 590–593. (b) Fischer, A.; Franco, A.; Oberholzer, T. *ChemBioChem* **2002**, *3*, 409–417. (c) Kita, H.; Matsuura, T.; Sunami, T.; Hosoda, K.; Ichihashi, N.; Tsukada, K.; Urabe, I.; Yomo, T. *ChemBioChem* **2008**, *9*, 2403–2410.

(24) Long, M. S.; Jones, C. D.; Helfrich, M. R.; Mangeney-Slavin, L. K.; Keating, C. D. *Proc. Natl. Acad. Sci. U.S.A.* **2005**, *102*, 5920–5925.

(25) Long, M. S.; Cans, A.-S.; Keating, C. D. *J. Am. Chem. Soc.* **2008**, *130*, 756–762.

(26) Helfrich, M. R.; Mangeney-Slavin, L. K.; Long, M. S.; Djoko, K. Y.; Keating, C. D. *J. Am. Chem. Soc.* **2002**, *124*, 13374–13375.
(27) Cans, A.-S.; Andes-Koback, M.; Keating, C. D. *J. Am. Chem. Soc.* **2008**, *130*, 7400–7406.
(28) Dominak, L. M.; Gundermann, E. L.; Keating, C. D. *Langmuir* **2010**, *26*, 5697–5705.
(29) (a) *Microcompartmentation and Phase Separation in Cytoplasm*; Walter, H., Brooks, D. E., Srere, P. A.; Eds.; International Review of Cytology; Academic Press: San Diego, 2000; Vol. 192. (b) Kerfeld, C. A.; Heinhorst, S.; Cannon, G. C. *Annu. Rev. Microbiol.* **2010**, *64*, 391–408. (c) Collier, J.; Shapiro, L. *Curr. Opin. Biotechnol.* **2007**, *18*, 333–340. (d) Yeates, T. O.; Kerfeld, C. A.; Heinhorst, S.; Cannon, G. C.; Shively, J. M. *Nat. Rev.* **2008**, *6*, 681–691.
(30) Wu, J.-Q.; Pollard, T. D. *Science* **2005**, *310*, 310–314.
(31) An, S.; Kumar, R.; Sheets, E. D.; Benkovic, S. J. *Science* **2008**, *320*, 103–106.
(32) Campanella, M. E.; Chu, H.; Low, P. S. *Proc. Natl. Acad. Sci. U.S.A.* **2005**, *102*, 2402–2407.
(33) Chen, Y. E.; Tropini, C.; Jonas, K.; Tsokos, C. G.; Huang, K. C.; Laub, M. T. *Proc. Natl. Acad. Sci. U.S.A.* **2011**, *108*, 1052–1057.
(34) (a) Tajbakhsh, S.; Rocheteau, P.; Le Roux, I. *Annu. Rev. Cell Dev. Biol.* **2009**, *25*, 671–699. (b) Horvitz, H. R.; Herskowitz, I. *Cell* **1992**, *68*, 237–255.
(35) Knoblich, J. A. *Nat. Rev. Mol. Cell Biol.* **2010**, *11*, 849–860.
(36) Drubin, D. G.; Hames, B. D.; Glover, D. M. *Cell Polarity: Frontiers in Molecular Biology*;Oxford University Press: New York, 2000.
(37) Liu, B.; Larsson, L.; Caballero, A.; Hao, X.; Öling, D.; Grantham, J.; Nyström, T. *Cell* **2010**, *140*, 257–267.
(38) Neumüller, R. A.; Knoblich, J. A. *Genes Dev.* **2009**, *23*, 2675–2699.
(39) Harold, F. M. *Microbiol. Mol. Biol. Rev.* **2005**, *69*, 544–564.
(40) Albertsson, P. A. *Partition of Cell Particles and Macromolecules*, 2nd ed.; Wiley-Interscience: New York, 1971.
(41) Walter, H.; Johansson, G. *Methods Enzymol.* **1994**, 228.
(42) Zaslavsky, B. Y. *Aqueous Two-Phase Partitioning: Physical Chemistry and Bioanalytical Applications*; Marcel Dekker: New York, 1995.
(43) *Aqueous Two-Phase Systems: Methods and Protocols*; Hatti-Kaul, R., Ed.; Methods in Biotechnology; Humana Press: New Jersey, 2000; Vol. 11.
(44) (a) Zhou, H.-X.; Rivas, G.; Minton, A. P. *Annu. Rev. Biophys.* **2008**, *37*, 375–397. (b) Ellis, R. J. *Trends Biochem. Sci.* **2001**, *26*, 597–604. (c) Johansson, H.-O.; Brooks, D. E.; Haynest, C. A. *Int. Rev. Cytol.* **1999**, *192*, 155–170. (d) Minton, A. P. *Curr. Biol.* **2006**, *16*, R269–R271.
(45) Yoon, Y.-Z.; Hale, J. P.; Petrov, P. G.; Cicuta, P. *J. Phys.: Condens. Matter* **2010**, *22*, 062101.
(46) (a) Veatch, S. L.; Polozov, I. V.; Gawrisch, K.; Keller, S. L. *Biophys. J.* **2004**, *86*, 2910–2922. (b) Veatch, S. L.; Keller, S. L. *Phys. Rev. Lett.* **2002**, *89*, 268101–268101−4.
(47) (a) Baumgart, T.; Hess, S. T.; Webb, W. W. *Nature* **2003**, *425*, 821–824. (b) Baumgart, T.; Das, S.; Webb, W. W.; Jenkins, J. T. *Biophys. J.* **2005**, *89*, 1067–1080.
(48) Because of some variation in the specific polymer compositions encapsulated by each vesicle,[16] we see some variability in partitioning as well as in the osmolality required for budding and fission for individual vesicles even within a single batch.[25,28]
(49) The osmolality of the PEG-rich phase was 115 ± 2.9[50] when freshly prepared and increased to 136 ± 1.2 after incubation under parafilm at 42 °C for 2−3 days to form vesicles; thus even without addition of sucrose the external solution was hypertonic with respect to the solution encapsulated within the vesicles.
(50) Vapor pressure osmometry measurements were performed at room temperature (25 °C). For the PEG-rich phase of the ATPS, measurements at this temperature will overestimate the osmolality under our experimental conditions (4 °C) by on the order of 10% or more;[51] thus, these values are most useful in a comparative rather than absolute sense.
(51) Stanley, C. B.; Strey, H. H. *Macromolecules* **2003**, *36*, 6888–6893.
(52) The initial addition of 130 mM sucrose led to a decrease in measured osmotic pressure, due to the nonadditive effect of multiple solutes on osmolality.[53] This did not alter the budded geometry of the vesicles, presumably because the total interior polymer concentration was on average lower in the ATPS from which the vesicles were formed.[16] Further aliquots of sucrose at increasing concentrations led to increased osmolality and the observed morphological changes leading to fission.
(53) Elliot, J. A. W.; Prickett, R. C.; Elmoazzen, H. Y.; Porter, K. R.; McGann, L. E. *J. Phys. Chem. B* **2007**, *111*, 1775–1785.
(54) (a) Karlsson, M.; Davidson, M.; Karlsson, R.; Karlsson, A.; Bergenholtz, J.; Konkoli, Z.; Jesorka, A.; Lobovkina, T.; Hurtig, J.; Voinova, M.; Orwar, O. *Annu. Rev. Phys. Chem.* **2004**, *55*, 613–49. (b) Hurtig, J.; Chiu, D. T.; Önfelt, B. *Wiley Interdiscip. Rev: Nanomed. Nanobiotechnol.* **2010**, *2*, 260–276.
(55) Waugh, R. E. *Biophys. J.* **1982**, *38*, 29–37.
(56) Evans, E.; Bowman, H.; Leung, A.; Needham, D.; Tirrell, D. *Science* **1996**, *273*, 933–935.
(57) Raucher, D.; Sheetz, M. P. *Biophys. J.* **1999**, *77*, 1992–2002.
(58) Roux, A.; Cappello, G.; Cartaud, J.; Prost, J.; Goud, B.; Bassereau, P. *Proc. Natl. Acad. Sci. U.S.A.* **2002**, *99*, 5394–5399.
(59) Heinrich, M.; Tian, A.; Esposito, C.; Baumgart, T. *Proc. Natl. Acad. Sci. U.S.A.* **2010**, *107*, 7208–7213.
(60) Sorre, B.; Callan-Jones, A.; Manneville, J.-B.; Nassoy, P.; Joanny, J.-F.; Prost, J.; Goud, B.; Bassereau, P. *Proc. Natl. Acad. Sci. U.S.A.* **2009**, *106*, 5622–5626.
(61) Li, Y.; Lipowsky, R.; Dimova, R. *Proc. Natl. Acad. Sci. U.S.A.* **2011**, *108*, 4731–4736.
(62) Allain, J.-M.; Storm, C.; Roux, A.; Amar, M. B.; Joanny, J.-F. *Phys. Rev. Lett.* **2004**, *93*, 158104–1- 158104−4.
(63) Roux, A.; Cuvelier, D.; Nassoy, P.; Prost, J.; Bassereau, P.; Goud, B. *EMBO J.* **2005**, *24*, 1537–1545.
(64) (a) Bar-Ziv, R.; Moses, E. *Phys. Rev. Lett.* **1994**, *73*, 1392–1395. (b) Bar-Ziv, R.; Tlusty, T.; Moses, E. *Phys. Rev. Lett.* **1997**, *79*, 1158–1161.
(65) Chaïeb, S.; Rica, S. *Phys. Rev. E* **1998**, *58*, 7733–7737.
(66) Tsafrir, I.; Sagi, D.; Arzi, T.; Guedeau-Boudeville, M.-A.; Frette, V.; Kandel, D.; Stavans, J. *Phys. Rev. Lett.* **2001**, *86*, 1138–1141.
(67) Yu, Y.; Granick, S. *J. Am. Chem. Soc.* **2009**, *131*, 14158–14159.
(68) Pullarkat, P. A.; Dommersnes, P.; Fernández, P.; Joanny, J.-F.; Ott, A. *Phys. Rev. Lett.* **2006**, *96*, 048104–1−048104−4.
(69) Liu, H.; Bachand, G. D.; Kim, H.; Hayden, C. C.; Abate, E. A.; Sasaki, D. Y. *Langmuir* **2008**, *24*, 3686–3869.
(70) Sackmann, E. *J. Phys.: Condens. Matter* **2006**, *18*, R785–R825.
(71) Peter, B. J.; Kent, H. M.; Mills, I. G.; Vallis, Y.; Butler, P. J. G.; Evans, P. R.; McMahon, H. T. *Science* **2004**, *303*, 495–499.
(72) Itoh, T.; Erdmann, K. S.; Roux, A.; Habermann, B.; Werner, H.; De Camili, P. *Dev. Cell* **2005**, *9*, 791–804.
(73) Farsad, K.; Ringstad, N.; Takei, K.; Floyd, S. R.; Rose, K.; De Camili, P. J. *Cell Biol.* **2001**, *155*, 193–200.
(74) Chou, T.; Jaric, M. V.; Siggia, E. D. *Biophys. J.* **1997**, *72*, 2042–2055.
(75) Helfrich, M. R.; El-Kouedi, M.; Etherton, M. R.; Keating, C. D. *Langmuir* **2005**, *21*, 8478–8486.
(76) Cavalier-Smith, T. *Trends Plant Sci.* **2000**, *5*, 174–182.
(77) In the initial images (far left panels), green fluorescence corresponding to the labeled streptavidin on the L_o lipid is visible between the PEG-rich and dextran-rich ends of the mother vesicle. We see membrane accumulation between the two aqueous phases under hypertonic conditions for some vesicles[28] and cannot be sure whether this indicates a barrier to diffusion between the two aqueous domains. Work by Li and Dimova suggests that this material is lipid nanotubes,[61] which would not seal off the two aqueous compartments. Our data do not enable us to make a distinction for this vesicle.
(78) Clark, J. I.; Clark, J. M. *Int. Rev. Cytol.* **2000**, *192*, 171–187.

(79) Brangwynne, C. P.; Eckmann, C. R.; Courson, D. S.; Rybarska, A.; Hoege, C.; Gharakhani, J.; Jülicher, F.; Hyman, A. A. *Science* **2009**, *324*, 1729–1732.
(80) Ge, X.; Conley, A. J.; Brandle, J. E.; Truant, R.; Filipe, C. D. M. *J. Am. Chem. Soc.* **2009**, *131*, 9094–9099.
(81) (a) Jacobson, K.; Mouritsen, O. G.; Anderson, R. G. W. *Nat. Cell Biol.* **2007**, *9*, 7–14. (b) Hancock, J. F. *Nat. Rev. Mol. Cell Biol.* **2006**, *7*, 456–462. (c) Coskun, U.; Simons, K. *FEBS Lett.* **2010**, *584*, 1685–1693. (d) Honerkamp-Smith, A. R.; Veatch, S. L.; Keller, S. L. *Biochim. Biophys. Acta* **2009**, *1788*, 53–63.
(82) (a) Stano, P.; Luisi, P. L. *Chem. Commun.* **2010**, *46*, 3639–3653. (b) Hanczyc, M. M.; Szostak, J. W. *Curr. Opin. Chem. Biol.* **2004**, *8*, 660–664.
(83) Kurihara, K.; Takakura, K.; Suzuki, K.; Toyota, T.; Sugawara, T. *Soft Matter* **2010**, *6*, 1888–1891.
(84) Zhu, T. F.; Szostak, J. W. *J. Am. Chem. Soc.* **2009**, *131*, 5705–5713.
(85) Akashi, K.-I.; Miyata, H.; Itoh, H.; Kinosita, K., Jr. *Biophys. J.* **1996**, *71*, 3242–3250.